Fabrication of macro-mesoporous zirconia-alumina materials with a 1D hierarchical structure

Erming Liu[□], Ashley J. Locke[□], Wayde N. Martens[□], Ray L. Frost[*, □], Xuzhuang Yang[†]

Discipline of Chemistry, Faculty of Science and Technology, Queensland University of Technology, GPO Box 2434, Brisbane Queensland 4001, Australia and College of Chemistry and Chemical Engineering, Inner Mongolia University, Huhhot, 010020, P.R. China

KEYWORDS: one dimensional (1D) nanocomposites, zirconia/alumina, nanorods, macroporous material, hierarchical structure

Abstract: A series of one dimensional (1D) zirconia/alumina nanocomposites were prepared by the deposition of zirconium species onto the 3D framework of boehmite nanofibres formed by dispersing boehmite nanofibres into butanol solution. The materials were calcined at 773K and characterized by X-ray diffraction (XRD), scanning electron microscopy (SEM), transmission electron microscope (TEM), N2 adsorption/desorption, infrared emission spectroscopy (IES). The results demonstrated that when the molar percentage X=100*Zr/(Al+Zr) was > 30 %, extremely long ZrO_2/Al_2O_3 composite nanorods with evenly distributed ZrO_2 nanocrystals on the surface were formed. The stacking of such nanorods gave rise to a new kind of macroporous material without the use of any organic space filler\template or other specific technologies. The mechanism for the formation of long ZrO_2/Al_2O_3 composite nanorods was proposed in this work.

Introduction

Inorganic metal oxides with macroporous frameworks usually possess very high relative pore volume and low apparent densities. Such materials are potentially useful in applications such as catalysis[1, 2], separation technology[3] and biomaterials engineering[4-6]. For instance, in macroporous catalysts the diffusion rate of small molecules can approach rates comparable to those in an open medium[7], and thereby greatly improve catalytic activity due to the enhanced diffusion of reactants and products[8].

Macroporous frameworks have been synthesized by two strategies, the first uses expensive organic templates, such as latex spheres or block-copolymers, which produce ordered networks usually unnecessary for the most catalytic reactions. The second is to combine sol-gel methods with a complicated drying technique, such as freeze-drying or supercritical drying[9]. The use of organic templates, such as latex spheres or block-copolymers, to control the structure of inorganic solids has proven to be a very successful strategy[10-12]. However, with this technique there is a need to remove the organic space fillers by calcination which usually occurs in flowing air at high temperature. This results in the emission of template decomposition gases and requires a large amount of energy, which on an industrial scale, may restrict its application due to stringent emission regulations and financial constraints. The high temperature required to remove the template may also cause structural collapse due to phase transformation and crystal growth. This is especially problematic for some transition metal oxides, such as ZrO_2. The second strategy usually involves complex procedures, which makes it difficult for scaling-up to practical applications[13].

To address these drawbacks, we designed a new strategy to prepare inorganic porous material by using a 1D nanomaterial, specifically AlOOH (boehmite) nanofibres, as a skeleton support. This is because the AlOOH nanofibres can be highly dispersed in liquid solutions to form a gel-like network (3D network)[14], which is readily accessible for the infiltration of active components or even small nanocrystallites. This allows the network to bear an extremely large loading on the surface, and theoretically allows for an even distribution of active components when compared with other traditional supports. After separation from liquid solution, nanocomposites can be stacked together with a very high pore volume due to their 1D architecture. Because of these large loading ratios, the properties of the active components will not be compromised by the interaction with alumina support after calcination[15]. Based on this consideration and given the good textural stability of alumina, using alumina nanofibres as hard template highlights a new opportunity to fabricate macroporous frameworks of some transition metal oxides with enhanced thermal and mechanical stability.

In this work, zirconium dioxide has been chosen to demonstrate our technique. Our interest in zirconia stems from its attractiveness as a catalyst and catalyst support which is used in many industrial processes[16-18]. It is also an important ceramic material exhibiting enhanced corrosion and oxidation resistance[19], fracture toughness[20], abrasion resistance[21], and excellent

[*] Author to whom correspondence should be addressed (r.frost@qut.edu.au)
P:+61 7 3138 2407 F:+61 7 3138 1804
[□] Queensland University of Technology
[†] Inner Mongolia University

biocompatibility when used in medical applications[22, 23]. For example, the material can be used as active support in three-way catalysts[24, 25] or to fabricate ceramic filter as well as thermal barrier. We prepared a series of ZrO_2/Al_2O_3 nanocomposites by depositing various amounts of zirconium species onto a three dimensional framework to form an extremely long ZrO_2/Al_2O_3 composite nanorods with a new core-shell structure, where a layer of tetragonal zirconia nanocrystallites shell was supported on long bundles of alumina nanofibres. The structures and physicochemical properties of resultant nanocomposites were characterized by means of XRD, SEM, TEM, IES, and the N_2 adsorption/desorption isotherms.

Experimental section

Materials. Boehmite fibres were synthesized by steam-assisted solid wet-gel method according to previous reports[26]. Butanol was purchased from Ajax Finechem and zirconium (IV) butoxide (80 wt. % in 1-butanol) was purchased from Aldrich. All these chemicals were used as received.

Nanocomposite preparation. 1D zirconia-boehmite nanocomposites were synthesized by the deposition of a zirconia species onto the boehmite nanofibres. In a typical procedure, 0.39 g of boehmite nanofibres was added to 0.20 g of deionised water, which was then dispersed into 20 ml of butanol with stirring. This mixture was then stirred for 24 hours to ensure complete dispersion of the nanofibers. The white suspension transformed into a translucent and highly viscous gel during the stirring process. Zirconium (IV) butoxide was dissolved into the resultant mixture according to the molar ratios X=100*Zr/(Al+Zr) = 5%, 10%, 15%, 30%, with stirring for 5~10 min. The synthesis procedure for the nanocomposite with molar ratio X= 50% was slightly different. Since the hydrolysis of zirconium butoxide consumes more water for this sample, the 0.39g of boehmite nanofibres were added into 0.40g deionised water. Subsequently, the viscous fluids were transferred into autoclaves for hydrothermal treatment at 170 °C for 24 hours. After cooling to room temperature, the resulting nanocomposites were separated by centrifugation (if the products were too sticky to transfer, acetone was added to enable the transfer), and then without any washing the samples were dried at 80 °C for 1 day, and labeled as Zr-m, where m is molar percentage of Zr. The calcined samples are labeled as Zr-"m"-T where T is calcination temperature.

The preparation of pristine ZrO_2 solid was accomplished by hydrolysis of zirconium butoxide dissolved in butanol with the addition of stoichiometric excess water. The resultant precipitate was calcined at 500 °C for 3 hours. The Al_2O_3 nanofibre sample was obtained by calcining neat boehmite nanofibres at 500 °C for 3 hours. These two materials would be used as reference materials to which a comparison can be made in the subsequent characterization.

Characterization. *XRD* patterns were collected on a PANalytical X'Pert PRO X-ray diffractometer (radius: 240.0 mm). Incident X-ray radiation was produced from a line-focused PW3373/10 Cu X-ray tube, operating at 40kV and 40mA, providing a Kα_1 wavelength of 1.540596 Å. The incident beam passed through a 0.04 rad Soller slit, a ½ divergence slit, a 15mm fixed mask, and a 1° fixed antiscatter slit. After interaction with the sample, the diffracted beam was detected by an X'Celerator RTMS detector, which was set in scanning mode, with an active length of 2.022mm. Diffraction patterns for the samples were collected over a rage of 3° ~ 75° 2θ. Reitveld refinement of XRD results was undertaken using a PANalytical Highscore Pluse software from Panalytical. *Surface Area Analysis* based on N_2 adsorption/desorption techniques were analysed on a Micrometrics Tristar 3000 automated gas adsorption analyser. Samples were pretreated at 200°C under the flow of N_2 for a minimum of 5 h on a Micrometrics Flowprep 060 degasser. *SEM micrographs* were obtained on a FEI QUANTA 200 scanning electron microscope operating at 30kV accelerating voltage with a 2.5 spot sizes. The samples were dried at room temperature and coated with gold under vacuum conditions in an argon atmosphere ionization chamber to increase surface conductivity. *FT-IR emission spectroscopy* was carried out on a Nicolet spectrometer but modified by replacing the IR source with an emission cell. The description of the cell and principles of the emission experiment have been published elsewhere[27]. *Transmission electron microscopy was* carried out on a Phillips Tecnai F20 TEM. The instrument was equipped with a Field Emission Gun source operating at a High Tension of 200 kV.

Results and Discussion

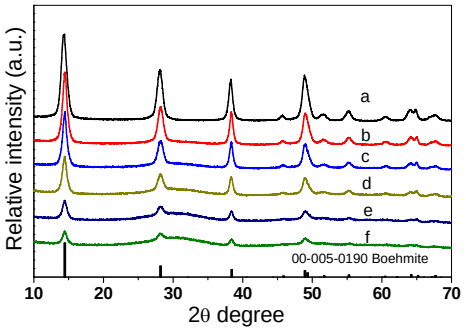

Figure 1. XRD patterns of composite nanofibres (a) pristine boehmite nanofibres, (b) Zr-5 (Zr%=5 mol%), (c) Zr-10 (Zr%=10 mol%), (d) Zr-15 (Zr%=15 mol%), (e) Zr-30 (Zr%=30 mol%), (f) Zr-50 (Zr%=50 mol%)

X-Ray Diffraction. X-Ray Diffraction was used to characterize crystalline phases of the zirconia on boehmite nanofibres. As seen in Figure 1, XRD signal of pristine boehmite nanofibres matched the peak positions of orthorhombic AlOOH (γ-AlOOH, JCPDS 00-005-0190). For as-synthesized nanocomposites, when the Zr molar percentage was below 5%, the XRD patterns of samples were almost identical to that of pristine boehmite nanofibres. When the Zr percentage was increased above 10%, a broad feature between 2θ=20° ~ 37° could be observed, which was ascribed to the diffractions of amorphous material, likely zirconia, since the intensity of this "hump" in-

* Author to whom correspondence should be addressed (r.frost@qut.edu.au)
P:+61 7 3138 2407 F:+61 7 3138 1804
□ Queensland University of Technology
† Inner Mongolia University

creases with increasing zirconia content, while the diffraction peaks corresponding to the boehmite nanofibres were weakened gradually.

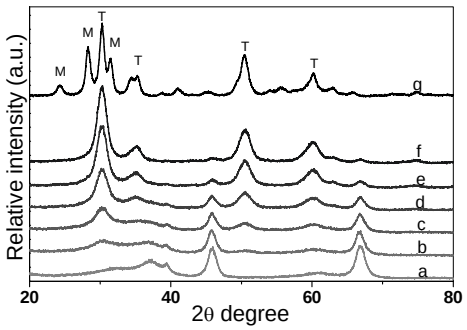

Figure 2. Powder XRD patterns of a) Al_2O_3 nanofibres; b) Zr-5-500; c) Zr-10-500; d) Zr-15-500; e) Zr-30-500; f) Zr-50-500; g) Pristine ZrO2 (M and T represent monoclinic ZrO_2 and tetragonal ZrO_2 respectively)

The XRD patterns for the nanocomposites calcined at 500°C are given in Figure 2. It is evident that the nanocomposites based on boehmite nanofibres transformed into nanocomposites containing γ-Al_2O_3 during calcination, which is consistent with the previously published data[28]. In addition, it can also be observed that with increasing zirconium content, the intensities of the diffraction peaks of γ-Al_2O_3 gradually decrease and become almost undetectable at 50 mol% Zr. This is due to the relative concentration of the alumina decreasing as well as the inherently poor intensity of peaks of the alumina[29]. As compared with pristine γ-Al_2O_3 nanofibres, the nanocomposite with 5% molar ratio shows a broadened peak at ca. 30° which increases in intensity with increasing zirconia content and can be confidently identified as the (101) plane of tetragonal zirconia when Zr molar percentage is above 15 %. No peak corresponding to monoclinic zirconia is observed in the patterns for all these nanocomposites. However, when pristine zirconia is calcined under the same conditions as the other samples, a small proportion of monoclinic zirconia is observed in addition to the tetragonal phase. This indicates that the transformation from the metastable tetragonal phase to the monoclinic phase is retarded when zirconium species are incorporated onto the surface of the alumina nanofibres.

The results of Rietveld refinements of the XRD data for these ZrO_2/Al_2O_3 nanocomposites are summarized in Table 1. The lattice parameters determined in this work show that the lattice constant of cubic γ-Al_2O_3, *a*, slightly increases with the addition of small amount of zirconium. In agreement with some literature reports[30], this indicates that Zr ions could be accommodated into the alumina structure. In contrast, the lattice constant of the tetragonal zirconia seemed to remain constant as the Zr percentage varied from 15 % to 50 %; however, when compared with pristine zirconia, the cellages of the as-synthesized nanocomposites do exhibit a decrease in tetragonality (*c*/*a* ratio), which shows the impregnation of aluminium atoms is not possible past an initial amount[31].

Table 1. Lattice parameters evolvement of γ-Al_2O_3 phase and tetragonal zirconia phase for the calcined sample with various Zr/Al molar ratios

Sample	γ-Al_2O_3 phase (cubic)			Zirconia nanocrystallite (tetragonal)		
	a[Å]	*b*[Å]	*c*[Å]	*a*[Å]	*b*[Å]	*c*[Å]
Al_2O_3 nanofibres	7.918±6	7.918±6	7.918±6	—	—	—
Zr-5-500	7.929±8	7.929±8	7.929±8	—	—	—
Zr-10-500	—	—	—	—	—	—
Zr-15-500	—	—	—	3.603±3	3.603±3	5.15±3
Zr-30-500	—	—	—	3.601±3	3.601±3	5.13±3
Zr-50-500	—	—	—	3.601±2	3.601±2	5.12±1
Pristine ZrO_2	—	—	—	3.590±4	3.590±4	5.20±2

It is well known that monoclinic ZrO_2 is stable from room temperature up to 1000 °C, with it transforming into the tetragonal phase above 1170 °C[32]. Stabilized tetragonal zirconia can exist at ambient temperature, when prepared using certain methods, such as adding divalent or trivalent oxides into the pristine oxide, or simply preparing it by the low temperature calcination of zirconyl nitrate or precipitating it from zirconium aqueous solution under alkaline conditions. Therefore, the occurrence of high temperature phase has been accounted for the formation of a solid solution[33, 34] and possibly as a result of the increased stability from the small size crystallites i.e., that the tetragonal zirconia is favoured below a critical crystal size ≈300 nm[35].

The crystal sizes of tetragonal zirconia for all the samples including the pristine zirconia and ZrO_2-Al_2O_3 nanocomposites were calculated by the Scherrer equation and are listed in Table 2. As the zirconium molar percentage in the nanocomposite is increased from 10 % to 50 %, there is a resulting increase of crystal size from 2.1 nm to 4.8 nm in (101) direction, smaller than that of the pristine zirconia, which is 9.0 nm. These results also elucidate the role of the alumina nanofibres in helping to stabilize the tetragonal zirconia through a reduction of the crystallite size.

Table 2. Crystallite dimension in (101) direction of tetragonal phase for pristine zirconia and zirconia deposited on alumina nanofibres with various zirconia content (The data were derived from X-ray diffraction patterns).

Sample name	Peak position (2θ)	FWHM (2θ)	Crystallite dimensions(nm)
Pristine ZrO_2	30.25	0.92	9.0
Zr-100-500	30.22	1.73	4.8
Zr-50-500	30.22	2.01	4.1
Zr-20-500	30.26	2.56	3.2

* Author to whom correspondence should be addressed (r.frost@qut.edu.au)
P:+61 7 3138 2407 F:+61 7 3138 1804
□ Queensland University of Technology
† Inner Mongolia University

Zr-10-500	30.42	4.00	2.1

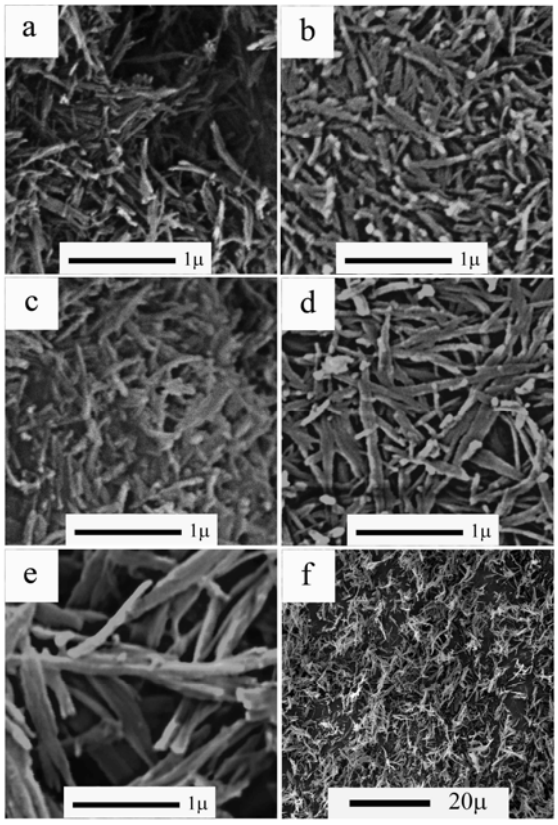

Figure 3. SEM images of 1D ZrO_2/Al_2O_3 nanocomposites obtained by calcination at 500°C: a) Zr-5-500; b) Zr-10-500; c) Zr-15-500; d) Zr-30-500; e) Zr-50-500; f) Zr-50-500 at a larger scale

Particle morphology was investigated by SEM and is illustrated in Figure 3. It can be observed that these nanocomposites undergo a macroscale morphological evolution with increasing Zr molar percentage. The zirconia species appear to be dispersed on single or small bundle of nanofibres. The continuity of zirconia coverage and the apparent structural integrity of the 1D nanocomposite fibres gradually increase as the zirconium content increases. As the Zr molar percentage is varied from 5 % to 15 %, the diameter of these 1D nanocomposites grows larger. A conspicuous change occurs when the Zr molar percentage is above 30%, the materials become extremely long and broad nanorods which are *ca.* 100 nm in width and average 1 micron in length for Zr-30-500 and 130 nm in width and average 2 microns in length for Zr-50-500. By convention, for a nano-fibrous material which consists of randomly stacked nanofibres, the resultant large intercrystallite voids are referred to as the porosity of such a material. Therefore, with the diameter of nanocomposite increasing, the inter-particle voids resulting from specific morphology of 1D nanomaterial are consequently extended. When the Zr molar percentage is above 30%, macropores in the range of 200 nm to 400 nm can be clearly observed. Especially for sample prepared with 50 mol% Zr, a distinct macroporous framework is fabricated from extremely long nanorods which are formed by the incorporation of several nanorods along the length direction (Figure 3f). This porous structure model is also supported by the results of N_2 adsorption/desorption experiments.

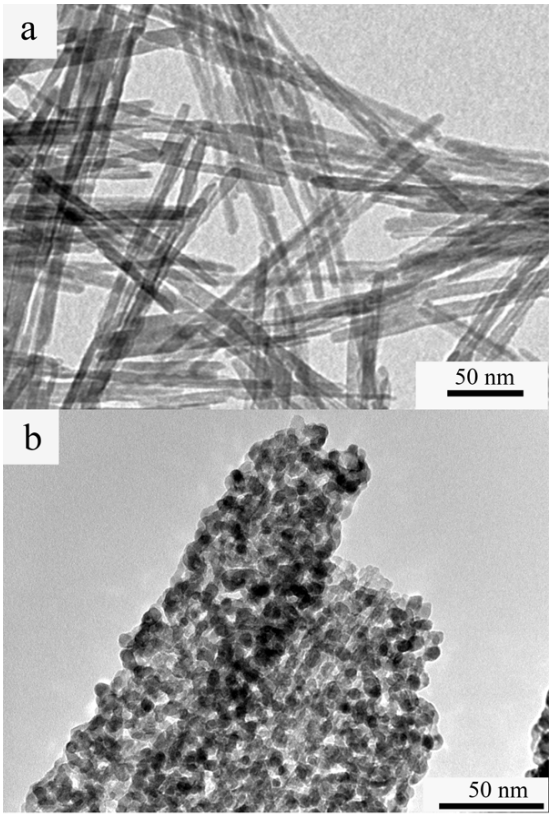

Figure 4. TEM image for γ-Al_2O_3 nanofibres and the 1D nanocomposite with 50 mol% Zr

Representative TEM images for γ-Al_2O_3 nanofibres and the 1D nanocomposite with 50 mol% Zr are shown in Figure 4. The γ-Al_2O_3 nanofibres are very thin and relatively short around 10~ 20 nm in diameter and 100~ 200 nm in length. However, the structure for the sample with 50 mol% Zr is significantly different: a great number of zirconia nanocrystallites can be easily identified by their dark contrast in the TEM, as a result of electron density contrast between Al and Zr[36]. The zirconia crystallites are about 5 nm, in agreement with calculations from XRD. These small nanoparticles, with interconnected architectures, form a relatively large porous nanorod.

* Author to whom correspondence should be addressed (r.frost@qut.edu.au)
P:+61 7 3138 2407 F:+61 7 3138 1804
 Queensland University of Technology
† Inner Mongolia University

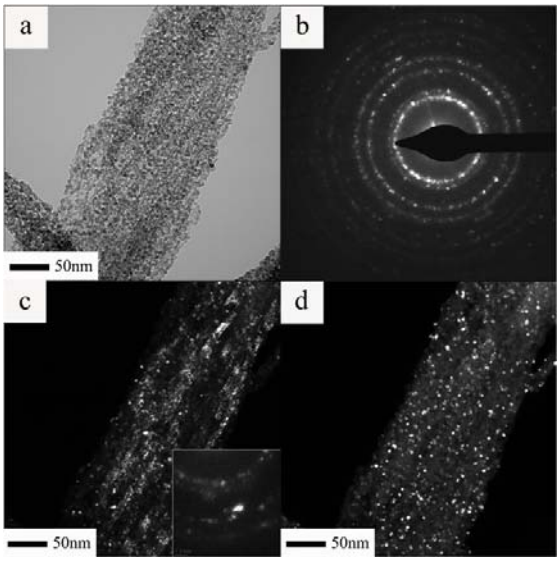

Figure 5. (a) Typical conventional TEM bright field, (b) the selected area electron diffraction pattern taken from same area, (c) the dark field image using the intensity of the (400) diffraction spot of γ-Al2O3 (shown as inset image) and (d) the dark field by selecting one of diffraction ring of zirconia for imaging

Moreover, typical TEM bright field and dark field images of this sample show more information on its structure. As the (400) diffraction spot of γ-Al_2O_3 is selected for imaging, the corresponding dark-field micrograph (Figure 5c) illustrates the location of alumina nanofibres, exhibiting relatively large bright areas with fibrous morphology which is congruent with a group of nanofibres connected together. It is worthy to mention here the electron beam which is diffracted off the (400) diffraction plane of alumina is required to pass through the layer of zirconia which diffracts this electron beam. This causes visible diffraction lines from the zirconia and causes mottling of the image. In contrast, when the dark-field image is taken using a tilt whose alignment is confluent with a diffraction spot of zirconia, a set of bright spots owing to the zirconia nanocrystallites, can be observed (Figure 5d), which also qualitatively indicates that the distribution of zirconia nanocrystallites is uniform. These two dark-field images strongly suggested that alumina nanorod core comprised of several oriented alumina nanofibers was encompassed by layered zirconia nanocrystallites.

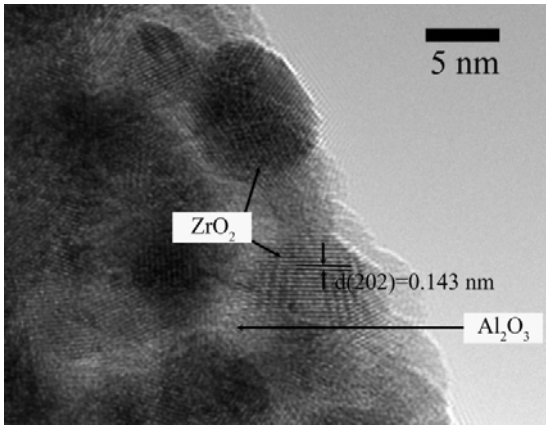

Figure 6. HRTEM image showing the embedment of ZrO_2 nanocrystallites on Al_2O_3 nanofibres

The strong interaction between γ-alumina and zirconia nanocrystallite is illustrated by HRTEM image (Figure 6). It shows that zirconia nanocrystallites are embedded on γ-Al_2O_3 support. The embedment on alumina support restricts advancing of crystal boundaries of zirconia, resulting in smaller crystal size for nanocomposites. Moreover, due to the large out-surface area of alumina nanofibres, separated zirconia nanocrystallites can also be observed. The relatively large distance between each zirconia nanocrystallite also prevents the coarsening of zirconia.

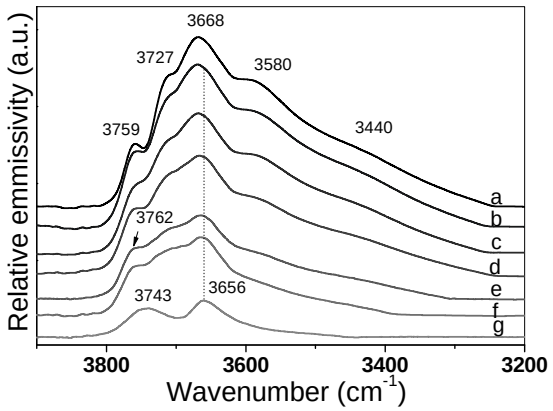

Figure 7. Infrared emission spectra in the region of OH stretching obtained at 400°C. a) γ-Al_2O_3 nanofibres, b) Zr-5-500, c) Zr-10-500, d) Zr-15-500, e) Zr-30-500, f) Zr-50-500, g) pristine ZrO_2

Figure 7 shows the Infrared Emission spectra (IES) for these nanocomposites in the hydroxyl stretching region. The spectrum for γ-Al_2O_3 nanofibres presents 5 typical bands which have been attributed to the different coordination (tetrahedral or octahedral) of the surface aluminum cations bonded to the hydroxyl group[37]. The two bands located at higher wavenumber, i.e. at 3759 and 3727 cm^{-1} correspond to isolated hydroxyl groups coordinated to one tetrahedral Al^{3+} and octahedral Al^{3+}, respectively. The bands at 3668 and 3580 cm^{-1} are attributed to the hydroxyl groups coordinated to two Al^{3+} ions with two subtypes: an octahedral aluminum ion with a tetrahedral alumi-

* Author to whom correspondence should be addressed (r.frost@qut.edu.au)
P:+61 7 3138 2407 F:+61 7 3138 1804
 Queensland University of Technology
† Inner Mongolia University

num ion and two octahedral aluminium ions. The band located at the lowest wavenumber corresponds to hydroxyl group coordinated to three Al^{3+} ions, i.e. two octahedral and one tetrahedral alumina[38]. Spectra of pristine ZrO_2 shows two hydroxyl stretches, located at 3743, and 3656 cm^{-1} which have been assigned to hydroxyl groups coordinated to two and three Zr^{4+} ions, respectively[39].

For ZrO_2/Al_2O_3 nanocomposites, the intensity of the hydroxyl bands corresponding to alumina decreased with increasing Zr molar percentage, indicating the alumina hydroxyls are sequentially replaced. The spectra of nanocomposites are very similar to that of γ-Al_2O_3, with the five types of alumina hydroxyl group being observed. This result is consistent with previous literature reports[30]. However, from low to high Zr molar percentage, there is a gradual band shift from 3668 to 3656 cm^{-1}, indicating the surface alumina hydroxyls have been replaced by the tribridged OH group of zirconia. It should be noted that the hydroxyl band at 3765 cm^{-1} assigned to isolated hydroxyl group coordinated to one Zr^{4+}, happens to coincide with the band for the isolated hydroxyl groups coordinated to one tetrahedral Al^{3+}, therefore, the band at 3762cm^{-1} should be assigned to isolated hydroxyl group of zirconia for these nanocomposites[39, 40]. Moreover, a broad shoulder in the 3692~ 3742 cm^{-1} range remains until a Zr molar percentage of 50 %, and may correspond to several different types of hydroxyl stretching deriving from alumina species interacted with Zr ions, which leads to the formation of practically unresolvable profile.

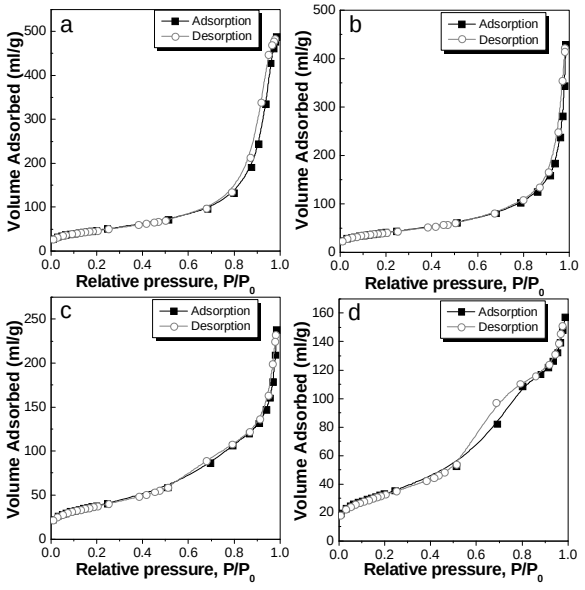

Figure 8. Nitrogen adsorption and desorption isotherms for some representative samples with various Zr molar percentage. a) γ-Al_2O_3 nanofibres, b) Zr-15-500, c) Zr-30-500, d) Zr-50-500

The surface area and pore structures of the samples are investigated by nitrogen adsorption-desorption isotherms. Figure 8 shows representative results to illustrate the textural changes as Zr content is increased. Pristine alumina nanofibres and all samples with Zr molar percentage up to 15 % exhibit similar adsorption-desorption isotherms with a hysteresis loop characteristic of capillary condensation, meaning the samples have a mesoporous nature. However, a distinct behavior can be perceived by the comparison of hysteresis loops. The hysteresis loop of the pristine alumina nanofibre falls within the H3 and H4 categories, which is typical of slit-type pores generated from the interparticle porosity of plate or fiber-like morphology[41]. The hysteresis loop for the Zr-15-500 sample exhibits a loop closer to that of the H3 destination, which shows a higher slope. According to Sing's study[42], H4 loop is attributed to narrow slit-like pores in the samples, therefore, such transformations in a hysteresis loop reflect the increase in the mean size of the slit-like pore.

Moreover, as the Zr molar percentage increases to 50 %, the isotherm takes a shape resembling a combination of Type II and IV adsorption. The adsorption branch of isotherm exhibits a capillary condensation step centered at relative pressure of about 0.67. Further to this at higher relative pressure, the nitrogen uptake dramatically increases and is sustained throughout entire pressure range. The desorption branch coincides with the adsorption branch until the relative pressure is lower than 0.8, where a hysteretic loop typical of a H2 was observed. This type of hysteresis is indicative of bottle ink pore networks[43]. This pore network is formed from the zirconia nanocrystallites, which has been confirmed by TEM (Figure 4). As the Isotherm is a combination of type II and IV absorption, it can be inferred that the nanocomposite material contains both meso- and macro- pores.

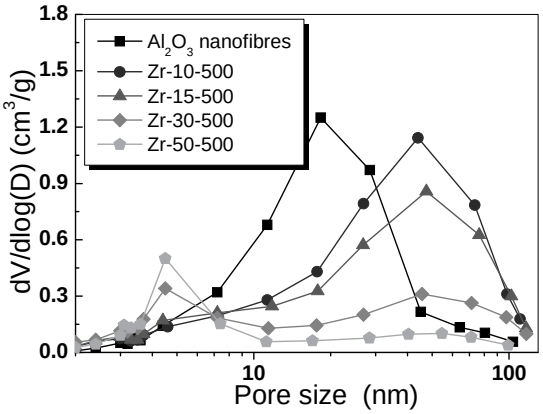

Figure 9. Pore size distributions for samples with various Zr molar percentage

Figure 9 illustrates the pore size distributions of representative samples. Alumina nanofibres have a wide pore size distribution from 1 nm to 100 nm, which is a characteristic feature of pores corresponding to the intercrystallites voids constituted by nanofibres. All nanocomposite samples show two pore distributions: one is 2-10 nm in size while the other is 10-100 nm in size. The former distribution is attributed to the pores formed by incorporation of zirconia nanocrystallites and the latter is assigned to those formed due to the 1D morphology of as-synthesized nanocomposites. It should be mentioned that an interesting phenomenon is observed, with increasing the zirconia content, the number of 2-10 nm pores increases due to the

* Author to whom correspondence should be addressed (r.frost@qut.edu.au)
P:+61 7 3138 2407 F:+61 7 3138 1804
Queensland University of Technology
† Inner Mongolia University

increase of zirconia nanocrystallites while the number of 10-100 nm pores decreases. When considered in light of the SEM results, this is because the inter-particle voids of the as-synthesized 1D nanocomposite have gradually extended to macropores of which the majority of the distribution exceeds the measurable range for N_2 physisorption. With increasing Zr molar percentage and the increase in diameter of fibrous nanocomposites, the number of large pores in the 10-100 nm range gradually decreases, which results into the decrease of average pore size and pore volume because these values are only calculated from the pores in the 2-100 nm range (Table 3).

Table 3. Pore structures of γ-Al_2O_3 nanofibres and as-synthesized nanocomposites

Sample	BET surface area(m^2/g)	Average pore size (nm)	Pore volume (cm^3/g)
γ-Al_2O_3 nanofibres	171	17.59	0.754
Zr-5-500	154	25.96	0.997
Zr-10-500	156	20.79	0.811
Zr-15-500	147	18.00	0.663
Zr-30-500	137	10.76	0.368
Zr-50-500	120	8.13	0.243
ZrO_2	44	17.60	0.196

Formation mechanism. In this work, we use thin boehmite (AlOOH) nanofibres as a hard-template to fabricate a series of ZrO_2/Al_2O_3 1D nanocomposites with an extremely large range of Zr molar percentage from 5% to 50%. Zirconia is deposited on boehmite nanofibres by the hydrolysis of zirconium butoxide followed by calcination at 500 °C. It is also demonstrated that when Zr molar percentage is above 30 %, the as-synthesized nanocomposites form a new class of 1D nanorods with large aspect ratio which can be easily constructed into macro-mesoporous materials without the use of a space filler or pore regulating agents.

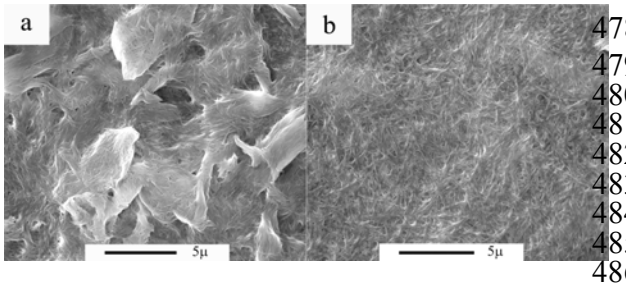

Figure 10. SEM images of thin films made from a) Dry boehmite nanofibres butanol suspension and b) wet boehmite nanofibres gel

The experiments show that the addition of water to boehmite nanofibres before their dispersion into butanol is essential to form the desired structure. Dry boehmite nanofibres can also be dispersed into butanol but without the formation of a viscous dispersion, while only wet boehmite nanofibres disperse into butanol forming a viscous translucent gel. To investigate the differences in the dispersive state, these two fluids were made into thin films on glass slides by the doctor-blade method. It can be observed (Figure 10) that the film made from dry boehmite nanofibres butanol suspension was constituted by large, uneven particles, indicating the dry boehmite nanofibres are dispersed by a flocculated aggregation in butanol. However, the film made from the wet boehmite nanofibre gel was constituted by numerous, evenly distributed, long bundles of boehmite nanofibres suggesting that a three-dimensional open grid is formed in gel-like fluid by cross-linked long bundles, and the mixture become viscous is also because of this[9]. These long bundles are very similar to the morphology of as-synthesized ZrO_2/Al_2O_3 composite nanorods with Zr percentage >30%.

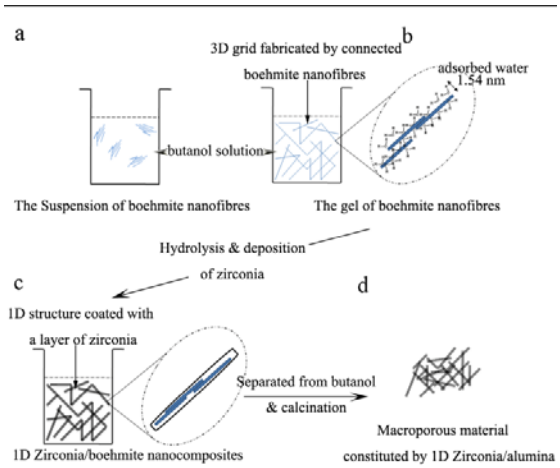

Figure 11. Schematic illustration of the formation mechanism of 1D zirconia/alumina nanocomposites and the macroporous material constituted by their 1D nanostructure: a) boehmite nanofibres are stabilized in butanol solution by forming an aggregated structure. b) 3D grid is formed by connected boehmite nanofibres. c) Zirconium butoxide is exclusively hydrolysed on the surface of boehmite nanofibres. d) 1D structure is maintained after separation and naturally packed into a macroporous material

Accordingly, the formation process is illustrated in Figure 11. It is worth mentioning here that since butanol is a hydrophobic alcohol, and the pre-adsorbed water on boehmite nanofibres will be immobilized on hydroxyl surface of boehmite crystallites in butanol dispersion. Obviously, such long bundles are directly formed from linear boehmite nanofibres which should be connected by the addition of water (Figure 11b). Subsequently, amorphous zirconia is precipitated onto the framework via the hydrolysis of zirconium butoxide at 170 °C, fixing this structure and forming a new class of 1D nanocomposite (Figure 11c). The hydrophobicity of butanol localizes the hydrolysis of zirconium butoxide onto the outer-surface of the boehmite nanofibres, rather than in the bulk liquid phase. Further, after separation from liquid phase, a macroporous framework with surface properties close to that of pristine zirconia will be inherently formed by the stacking of these nanorods as Zr molar higher than 30%.

* Author to whom correspondence should be addressed (r.frost@qut.edu.au)
P:+61 7 3138 2407 F:+61 7 3138 1804
□ Queensland University of Technology
† Inner Mongolia University

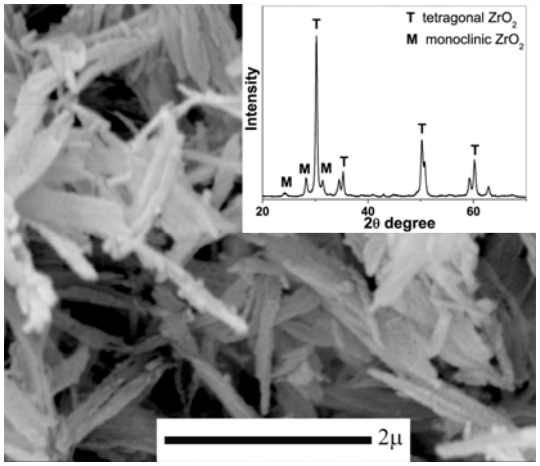

Figure 12. SEM image and XRD pattern for the sample with 50 % Zr molar percentage after calcination at 1000 °C

Advantages of the technique. Compared with a gel formed by nanoparticles, the network in boehmite nanofibres gel structure can be more easily conserved and consolidated as 1D nanocomposite. This is largely due to the random linkages between two orientated nanofibres can generate stronger interactions resulting from longer range contact when compared to that of isotropic nanoparticles. Therefore, there is no need for specific techniques during the preparation steps, such as, freeze drying or supercritical drying. This indicates that it is amenable to commercial scale-up.

Besides the benefit of a facilitated synthesis, compared with traditional macroporous materials, as-synthesized 1D nanocomposite also provides high thermal stability to the structure at the calcination temperature. This is illustrated in Figure 12 by SEM image and XRD pattern (inset image). After calcination at 1000 °C, for the sample with 50 % Zr molar percentage, the calculation from the XRD pattern shows the crystallite size of tetragonal zirconia dramatically increases at such a high temperatures, and at this temperature there is also the formation of some of monoclinic zirconia. However the alumina nanofibres maintained their morphology irrespective of crystallite growth and phase change of the zirconia, which is not achievable by a hierarchical material constructed by a pristine oxide. Moreover, after calcination at 1000 °C for 3 hours, the resultant material still possesses a relatively large surface area which is mainly determined by crystal size of zirconia (Table 4).

Table 4. Structure change for the sample with 50 % Zr molar percentage after calcining at 500 °C, 750 °C and 1000 °C for 3 hours

Sample name	Crystallite dimensions in (101) direction	BET surface area(m^2g-1)	Pore volume (cm^3/g)[b]
Zr-50-500	4.8	120	0.243
Zr-50-750	7.2	73	0.200
Zr-50-1000	21.4	28 [a]	0.113

[a] The surface area mainly contributed from the meso-pores formed by ZrO_2 nanocrystallites

[b] Macro-pores fabricated by the 1D nanocomposites are not detectable by N_2 physisorption

Conclusions

A series of 1D ZrO_2/Al_2O_3 nanocomposites with various Zr molar percentages from 5% to 50% were synthesized. It was demonstrate that zirconia macroporous materials can be fabricated using alumina nanofibres as hard-templates rather than using any space filler or pore-regulating agents. The incorporation of a large amount of zirconia nanocrystallites onto an alumina nanofibres framework also contributed new mesopores in the material, which results in a large surface area. In addition, the macroporous structures can be maintained irrespective of crystallite growth and phase change of zirconia when heated to 1000 °C.

The formation mechanism of the 1D ZrO_2/Al_2O_3 nanocomposite and relative zirconia macroporous material are proposed. When wet boehmite nanofibres are dispersed into butanol, these nanofibres link together to build up a 3D network on which a large amount zirconia (Zr molar percentage achieve 50%) can be deposited to prepare the 1D nanocomposite fibres. A macroporous material is naturally formed by the stacking of these large 1D nanocomposite fibres. An effective and green approach is offered to create a novel zirconia macroporous material with large surface area and high thermal stability.

Acknowledgements
The financial and infra-structure support from the Queensland University of Technology Chemistry Discipline is gratefully acknowledged. E.M.L is thankful for a Queensland University of Technology doctoral scholarship. One author is grateful for the finical support in the form of an Australia Post Doctoral Fellowship Provided by the Australian Research Council and a Smart State Fellowship provided by the Queensland State Government.

REFERENCES

(1) Landau, M. V.; Shter, G. E.; Titelman, L.; Gelman, V.; Rotter, H.; Grader, G. S.; Herskowitz, M., Alumina Foam Coated with Nanostructured Chromia Aerogel: Efficient Catalytic Material for Complete Combustion of Chlorinated VOC. *Ind. Eng. Chem. Res.* **2006,** 45, 7462-7469.

(2) Giani, L.; Crstiani, C.; Groppi, G.; Tronconi, E., Washcoating method for Pd/γ-Al_2O_3 deposition on metallic foams *Appl. Catal. B: Environ.* **2006,** 62, 121-131.

(3) Gestel, T. V.; Vandecasteele, C.; Buekenhoudt, A.; Dotremont, C.; Luyten, J.; Leysen, R.; Bruggen, B. V. d.; Maes, G., Alumina and titania multilayer membranes for nanofiltration: preparation, charcterization and chemical stability. *J. Membr. Sci.* **2002,** 207, 73-89.

(4) Ozin, G. A., Morphogenesis of Biomineral and Morphosynthesis of Biomimetic Forms. *Acc. Chem. Res.* **1997,** 30, 17-27.

* Author to whom correspondence should be addressed (r.frost@qut.edu.au)
P:+61 7 3138 2407 F:+61 7 3138 1804
□ Queensland University of Technology
† Inner Mongolia University

(5) Xu, H. H. K.; Quinn, J. B.; Takagi, S.; Chow, L. C. Synergistic reinforcement of in situ hardening calcium phosphate composite scaffold for bone tissue engineering. *Biomaterials* **2004,** 25, 1029-1037.

(6) Yuan, Z.; Su, B., Insights into hierarchically meso-macroporous structured materials. *J. Mater. Chem.* **2006,** 16, 663-677.

(7) Rolison, D. R., Catalytic Nanoarchitechtures--the importance of Nothing and Unimportance of Perodicity. *Science* **2003,** 299, 1698-1701.

(8) Yu, J.; Yu, J. C.; Leung, M. K.-P.; Ho, W.; BeiCheng; Zhao, X.; Zhao, J., Effects of acidic and basic hydrolysis catalysts on the photocatalytic activity and microstructures of bimodal mesoporous titania. *J. Catal.* **217,** 217, 69-78.

(9) Pierre, A. C.; Pajonk, G. M., Chemistry of Aerogels and Their Applications. *Chem. Rev.* **2002,** 102, 4243-4265.

(10) Holland, B. T.; Blanford, C. F.; Stein, A., Synthesis of Macroporous Minerals with Highly Ordered Three-Dimensional Arrays of Spheroidal Voids. *Science* **1998,** 281, 538-540.

(11) Davis, S. A.; Burkett, S. L.; Mendelson, N. H.; Mann, S., Bacterial templating of ordered macrostructures in silica and silica surfactant mesophases. *Nature* **1997,** 385, 420-423.

(12) Zhang, B.; Davis, S. A.; Mann, S., Starch Gel Templating of Spongelike Macroporous Silicalite Monoliths and Mesoporous Films. *Chem. Mater.* **2002,** 14, 1369-1375.

(13) Husing, N.; Schubert, U., Aerogels-Airy Materials: Chemistry, Structure, and Properties. *Angew. Chem. Int. Ed.* **1998,** 37, 22-45.

(14) Wierenga, A.; Philipse, A. P.; Lekkerkerker, H. N. W., Aqueous Dispersions of Colloidal Boehmite: Structure, Dynamics, and Yield Stress of Rod Gels. *Langmuir* **1998,** 14, 55-65.

(15) Korhonen, S. T.; Airaksinen, S. M. K.; Banares, M. A.; Krause, A. O. I., Isobutane dehydrogenation on zirconia-, alumina- and zirconia/alumina-supported chromia catalysts. *Appl. Catal. A: Gen.* **2007,** 333, 30-41.

(16) Korhonen, S. T.; Banares, M. A.; Fierro, J. L. G.; Krause, A. O. I., Adsorption of methanol as a probe for surface characteristics of zirconia-, alumina-, and zirconia/alumina-supported chromia catalysts. *Catal. Today* **2007,** 126, 235-247.

(17) Persson, K.; Ersson, A.; Colussi, S.; Trovarelli, A.; Jaras, S. G., Catalytic combustion of methane over bimetallic Pd-Pt catalysts: The influence of support materials. *Appl. Catal. B: Environ.* **2006,** 66, 175-185.

(18) Lefferts, L.; Seshan, K.; Mojet, B.; Ommen, J. v., Non-conventional oxidation catalysis. *Catal. Today* **2005,** 100, 63-69.

(19) Miao, X.; Ben-Nissan, B., Microstructure and properties of zirconia-alumina naolaminate sol-gel coatings. *J. Mater. Sci.* **2000,** 35, 497-502.

(20) Choi, S. R.; Bansal, N. P., Mechanical behavior of zirconia/alumina composites. *Ceram. Int.* **2005,** 31, 39-46.

(21) Holand, W.; Rheinberger, V.; Apel, E.; Ritzberger, C.; Rothbrust, F.; Kappert, H.; Krumeich, F.; Nesper, R., Future perspectives of biomaterials for dental restoration. *J. Eur. Ceram. Soc.* **2009,** 29, 1291-1297.

(22) Kim, H.-W.; Shin, S.-Y.; Kim, H.-e.; Lee, Y.-M.; Chung, C. P.; Lee, H.-H.; Rhyu, I.-C., Bone Foration on the Apatite-coated Zirconia Porous Scaffolds within a Rabbit Calvarial Defect. *J. Biomater. Appl.* **2008,** 22, 485-504.

(23) Chevalier, J.; Gremillard, L., Ceramics for medical applications: A picture for the next 20 years. *J. Eur. Ceram. Soc.* **2009,** 29, 1245-1255.

(24) Moran-Pineda, M.; Castillo, S.; Lopez, T.; Gomez, R.; Cordero-Borboa; Novaro, O., Synthesis, characterization and catalytic acitivity in the reduction of NO by CO on alumina-zirconia sol-gel derived mixed oxides. *Appl. Catal. B: Environ.* **1999,** 21, 79-88.

(25) Tiznado, H.; Fuentes, S.; Zaera, F., Infrared Study of CO Adsorbed on Pd/Al_2O_3-ZrO_2. Effect of Zirconia Added by Impregnation. *Langmuir* **2004,** 20, 10490-10497.

(26) Shen, S. C.; Ng, W. K.; Chen, Q.; Zeng, X. T.; Chew, M. Z.; Tan, R. B. H., Solid-Phase Low Temperature Steam-Assisted Synthesis of Thermal Stable Alumina Nanowires. *J. Nanosci. Nanotechno.* **2007,** 7, 2726-2733.

(27) Kloprogge, J. T.; Frost, R. L., Infrared emission spectroscopic study of the dehydroxylation of synthetic Mg/Al and Mg/Zn/Al-hydrotalcites. *Phys. Chem. Chem. Phys.* **1999,** 1, 1641-1647.

(28) Shen, S. C.; Chen, Q.; Chow, P. S.; Tan, G. H.; Zeng, X. T.; Wang, Z.; Tan, R. B. H., Steam-Assisted Solid Wet-Gel Synthesis of High-Quality Nanorods of Boehmite and Alumina. *J. Phys. Chem. C* **2007,** 111, 700-707.

(29) Li, G.; Li, W.; Zhang, M.; Tao, K., Characterization and Catalytic application of homogeneous nano-composite oxides ZrO_2-Al_2O_3. *Catal. Today* **2004,** 93-95, 595-601.

(30) Jr, A. C. F.; Souza, K. R.; Camorim, V. L. D. L.; Cardoso, M. B., Zirconia-alumina mixing in alumina-supported zirconia prepared by impregnation with solutions of zirconium acetylacetonate. *Phys. Chem. Chem. Phys.* **2003,** 5, 1932-1940.

(31) Muller, E.; Oestreich, C.; Klemm, V.; Brendler, E.; Ferkel, H.; Riehemann, W., Zirconia-Alumina Nanoparticles Prepared by Laser Evaporation: Powder Characterisation by TEM and ^{27}Al MAS NMR. *Part. Part. Syst. Charact.* **2002,** 19, 169-175.

(32) Jaenicke, S.; Chuah, G. K.; Raju, V.; Y, T. N., Structural and Morphological Control in the Preparation of High Surface Area Zirconia. *Catal. Surv. Asia* **2008,** 12, 153-169.

(33) Dongare, M. K.; Sinha, A. P. B., Low temperature preparation of stabilized zirconia. *J. Mater. Sci.* **1984,** 19, 49-56.

(34) Scott, H. G., Phase relationships in the zirconia-yttria system. *J. Mater. Sci.* **1975,** 10, 1527-1535.

(35) Garvie, R. C., The Occurrence of Metastable Tetragonal Zirconia as a Crystallite Size Effect. *J. Phys. Chem.* **1965,** 69, 1238-1243.

(36) Mokarl, T.; Sztrum, C. G.; Salant, A.; Rabani, E.; Banin, U., Formation of asymmetric one-sided metal-tipped semiconductor nanocrystal dots and rods. *Nature Mater.* **2005,** 4, 855-863.

(37) Knozinger, H.; Ratnasamy, P., Catalytic Aluminas: Surface Models and Characterization of Surface Sites. *Catal. Rev. Sci. Eng.* **1978,** 17, 31-70.

(38) Turek, A. M.; Wachs, I. E., Acidic Properties of Alumina-Supported Metal Oxide Catalysts: An Infrared Spectroscopy Study. *J. Phys. Chem.* **1992,** 96, 5000-5007.

(39) Jung, K. T.; Bell, A. T., The effects of synthesis and pretreatment conditions on the bulk structure and surface properties of zirconia. *J. Mol. Catal. A: Chem.* **2000,** 163, 27-42.

(40) Cerrato, G.; Bordiga, S.; Barbera, S.; Morterra, C., Surface characterzation of monoclinic ZrO_2 I. Morphology, FTIR spectral features, and computer modelling. *Appl. Surf. Sci.* **1997,** 115, 53-65.

(41) Martinez, A.; Prieto, G.; Rollan, J., Nanofibrous γ-Al_2O_3 as support for Co-based Fischer-Tropsch catalysts: Pondering the relevance of diffusional and dispersion effects on catalytic perfrmance. *J. Catal.* **2009,** 263, 292-305.

(42) Sing, K. S. W.; Everett, D. H.; Haul, R. A. W.; Moscou, L.; Pierotti, R. A.; Rouquerol, J.; Siemieniewska, T., Reporting physisorption data for Gas/Solid systems. *Pure & Appl. Chem.* **1985,** 57, 603-619.

(43) Kruk, M.; Jaroniec, M., Gas Adsorption Characterization of Ordered Organic-Inorganic Nanocomposite Materials. *Chem. Mater.* **2001,** 13, 3169-3182.

* Author to whom correspondence should be addressed (r.frost@qut.edu.au)
P:+61 7 3138 2407 F:+61 7 3138 1804
 Queensland University of Technology
† Inner Mongolia University

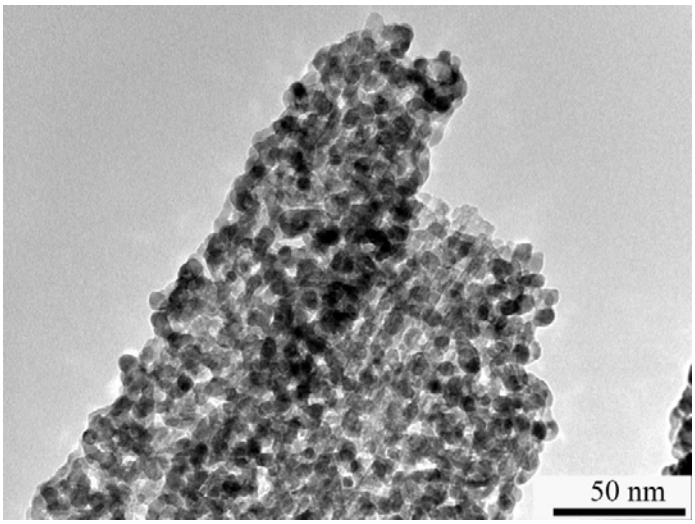

TEM image for the sample with 50% Zr molar percentage

Zirconia nanoparticles, identified by the dark contrast in the TEM due to its high electron density, are about 5nm. These nanoparticles encompass the out surface of alumina nanofibres, and with interconnected architectures form a porous nanorod. The stacking of such nanorods generates a new kind of macroporous material without the use of any organic space filler\template or other specific technologies.